

# Steel Ladle Slag Zone Lining Optimization Considering Irreversible Material Behavior

Maximilian Klopff,\* Aidong Hou, Shengli Jin, and Dietmar Gruber\*

The optimization of refractory linings is a complex task due to the many factors that influence the thermomechanical behavior. This study applies the multiparameter optimization method technique for order preference by similarity to the ideal solution to a commercially used slag zone lining of a secondary metallurgical steel ladle, considering the influence of different material models in a finite element (FE) simulation. The dataset is acquired by varying the working lining brick shape, initial expansion allowance (IEA), and isolation layer thickness. The maximum irreversible strain, joint opening at the hot face, and steel shell temperature are determined from the FE simulation results and used as the input values for the optimization. A larger circumferential brick dimension combined with low IEA is favorable for the von Mises creep model. The main contribution is from the IEA (98.53%). The optimized lining for the Drucker–Prager criterion has a brick with a small circumferential dimension and larger IEA. The main influencing factor is the brick shape (85.06%). The differences in the optimization results and factor contributions can be explained by the contribution of the constitutive models to the simulation results before and after the thermal shock.

and thermomechanical performance of steel ladle linings were evaluated extensively to investigate the lining concepts.<sup>[3–10]</sup> In previous studies, a ladle lining with typical structure was optimized using single-response and multiresponse optimization methods to prove the applicability of concepts considering elastic material behavior.<sup>[11–13]</sup> This study aims to optimize the thermomechanical behavior of a commercially used steel ladle slag zone lining using a multiresponse optimization technique, the technique for order preference by similarity to the ideal solution (TOPSIS). A lining database was compiled by varying the brick shape, initial expansion allowance (IEA), and isolation layer thickness (ILT). FE simulations, including irreversible material behavior, were performed to obtain the responses. Subsequently, the TOPSIS was used to convert multiple responses into a single response and rank

## 1. Introduction

Refractory-lined steel ladles play a crucial role in secondary metallurgy. Steel ladles are used as refining and transport vessels for molten steel, and are exposed to strongly varying operating conditions.<sup>[1,2]</sup> A well-designed steel ladle offers benefits in terms of steel quality, productivity, lifetime, and refractory consumption.<sup>[1,2]</sup> Various factors affect the performance of the steel ladles; therefore, the design and lining of optimization are complex. Using finite element (FE) simulations, the thermal

the linings according to their performance. A combination of optimal levels and factor contributions to the overall performance was determined using the signal-to-noise (S/N) ratio and analysis of variance (ANOVA).

## 2. Methodology


### 2.1. Case Study

For the case study, the slag zone lining of a commercially used steel ladle in secondary metallurgy was selected. The lining had a three-layer structure consisting of a 155 mm magnesia carbon (MgO-C) brick as the working lining (WL, brick 1), 70 mm of high-alumina castable as the permanent lining (PL), and 6 mm as the isolation layer (ISO), with an overall thickness of 261 mm, including a 30 mm steel shell (SS). The dimensions of brick shape 1 are outlined in Table 2. Based on the described slag zone lining and to reduce the computational costs by considering all the symmetries, a 3D unit cell model (Figure 1) of one-quarter of the original brick dimensions was created in the commercial finite element software ABAQUS<sup>[14]</sup> utilizing the coupled temperature–displacement element type C3D8T. An IEA of 0.2 mm in the circumferential direction was applied to the WL. This model is referred to below as the standard reference model. The ladle preheating and first-ladle heat, including the idle time, were simulated.

The ambient temperature of the refractory lining and the SS was set to 25 °C. The thermal boundary conditions for the

M. Klopff  
K1-MET GmbH  
8700 Leoben, Austria  
E-mail: maximilian.klopff@unileoben.ac.at

A. Hou, S. Jin, D. Gruber  
Montanuniversitaet Leoben, Chair of Ceramics  
8700 Leoben, Austria  
E-mail: dietmar.gruber@unileoben.ac.at

 The ORCID identification number(s) for the author(s) of this article can be found under <https://doi.org/10.1002/srin.202300557>.

© 2024 The Authors. Steel Research International published by Wiley-VCH GmbH. This is an open access article under the terms of the Creative Commons Attribution-NonCommercial-NoDerivs License, which permits use and distribution in any medium, provided the original work is properly cited, the use is non-commercial and no modifications or adaptations are made.

DOI: 10.1002/srin.202300557

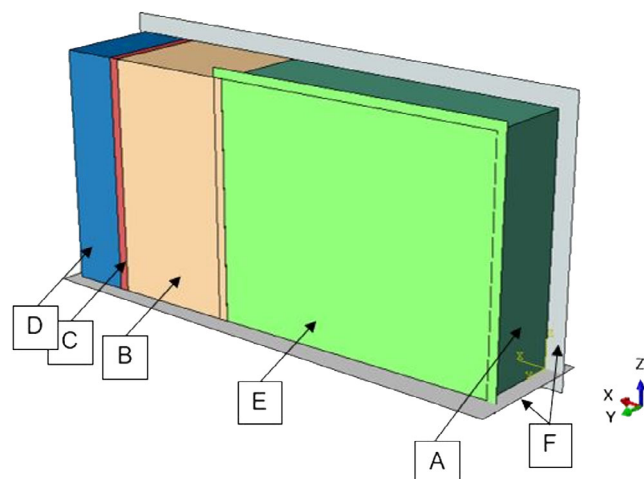


**Figure 1.** Steel ladle slag zone lining finite element unit cell model: A) WL, B) PL, C) ISO, D) SS, E) rigid plate, and F) symmetry planes.

simulation were based on the measurements performed using a commercial secondary steel ladle during service.<sup>[15]</sup> The measured temperature curves were used as reference, and the heat transfer conditions were modified to fit simulated temperatures (Figure 2). The simulated hot-face temperatures are shown in Figure 2. The ladle was preheated for 57 h up to a hot face (HF) temperature of 1000 °C. The decreases after 40 h and at

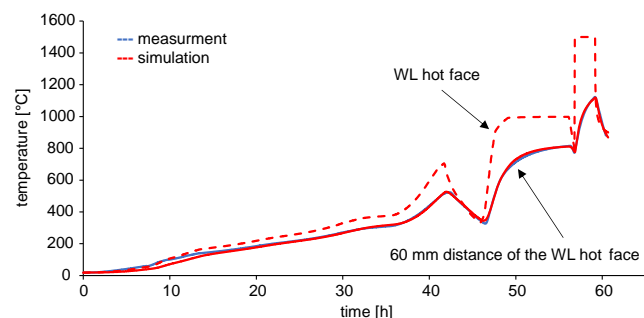


**Figure 2.** Simulated temperature on the WL HF and comparison of the measured and simulated temperature curve in 60 mm distance of the WL HF.

**Table 1.** Material properties of the MgO-C material, PL, ISO, and SS.

		MgO-C (WL)	PL	ISO	SS
Young's modulus [GPa]	$E$	31.6–51.2	20	0.17	210
Poisson's ratio	$\nu$	–0.2	0.2	0.2	0.3
Cohesion <sup>[25]</sup>	$d$	7–12.1 MPa	–	–	–
Friction angle <sup>[25]</sup>	$\beta$	63°	–	–	–
Dilatation angle	$\phi$	48.4°	–	–	–
Thermal expansion [ $K^{-1}$ ]	$\alpha$	$7.5 \times 10^{-6}$ – $1.06 \times 10^{-5}$	$7 \times 10^{-6}$	$6 \times 10^{-6}$	$1.2 \times 10^{-5}$
Conductivity [ $Wm^{-1} K^{-1}$ ]	$\lambda$	7.5	3	0.15	50
Specific heat [ $Jkg^{-1} K^{-1}$ ]	$C$	1000	1000	1000	1000
Density [ $kgm^{-3}$ ]	$\rho$	3070	2950	1000	7600

the end of preheating are caused by transports of the steel ladle in the steel mill. The heat lasted 2.4 h, the thermal shock was simulated with a temperature increase to 1600 °C in 120 s, followed by an idle time of 1.5 h. Conditions at the inner surface of the ladle were considered adiabatic during the idle time. The heat transfer from the SS to the ambient temperature was temperature-dependent, with the heat transfer coefficients calculated according to ref. [16].

The symmetry planes defining the unit cell model were modeled as symmetrical boundary conditions. The SS was mechanically constrained in the circumferential direction. The contacts between the lining layers and SS were modeled with the penalty method as frictionless hard contacts.<sup>[14]</sup> The temperature-dependent material properties of the resin-bonded MgO-C brick and the material properties of the PL, ISO, and SS are listed in Table 1. The applied Norton–Bailey compressive creep parameters of the MgO-C material are outlined in ref. [17]. The density, specific heat, conductivity, and thermal expansion were obtained from the datasheets. The MgO-C Poisson's ratio of –0.2 was measured at 25 °C using the impulse excitation technique with flexure and torsional waves.

The thermal and thermomechanical responses were obtained through coupled thermomechanical FE simulations. The Drucker–Prager yield criterion (DP)<sup>[18]</sup> and Norton–Bailey creep based on the von Mises stress (VMC)<sup>[14]</sup> were applied to consider the irreversible material behavior. The selected parameters for the optimization included the maximum irreversible strain in the circumferential direction ( $\epsilon_{ir}$ ), the joint opening at the HF at the end of preheating ( $x_{open}$ ), and the SS temperature on the outer surface at the end of the idle time ( $\vartheta_{ST}$ ).

## 2.2. Establishment of Lining Configuration Dataset

The process conditions and geometry influence the stress, strain, and temperature distribution in an industrial lining. To obtain lining configurations as a basis for the optimization, the WL brick shape, IEA, and ILT were varied, while the boundary conditions remained identical for all models.

The aforementioned FE model described is the standard reference model for optimization. First, the shape of the WL brick was varied to obtain different lining configurations.

Four different brick shapes were selected. The geometric parameters of the WL bricks are listed in Table 2. The overall

**Table 2.** Characterization of WL brick shapes and respective PL thickness in FE model.

Brick	WL thickness [mm] x-axis	WL HF width [mm] y-axis	WL CE width [mm] y-axis	WL height [mm] z-axis	PL thickness [mm] x-axis
1	155	95	105	250	70
2	124	120	130	250	101
3	187	94	106	250	38
4	152.4	140	154	100	72.6

lining thickness remained constant for all the FE models, and the PL thickness balanced the differences in the WL thickness. Brick 1 was used in the reference model. Bricks 2 and 3 were of the same height as the reference brick with lower and higher WL thicknesses, respectively. Brick 4 had a height of only 100 mm and WL thickness similar to that of Brick 1. This leads to four linings with different WL and PL dimensions and identical overall lining thickness.

For each FE model, utilizing the four WL bricks, the IEA and ILT were varied. Five different IEAs and ILTs were selected, resulting in 25 individual lining configurations per WL brick shape. In addition, the overall lining thickness remained constant. The size of the IEA was determined as a percentage of the WL HF width: 0.21%, 0.32%, 0.42%, 0.53%, and 0.63% defining the IEA, respectively. The actual IEA in millimeters for each FE model was calculated by multiplying the WL HF width by the respective defined percentages. The applied ILTs were 0, 3, 6, 9, and 12 mm. The difference in thickness was balanced by the PL thickness so that the overall lining thickness remained constant. The outlined procedure resulted in 100 different lining configurations and simulation results for each applied constitutive model.

A hexagonal mesh was used for all models. As the dimensions of the simulation models and lining sections vary considerably, the mesh sizes also vary. At the beginning of the study, a mesh optimization was carried out to find the optimum configurations. During the simulations, the mesh size was not changed, and the minimum mesh size used in the WL was 3 mm. For the standard reference model outlined, the mesh sizes were 3–7 mm for WL with smaller mesh sizes on the HF, 5 mm for PL and SS, 3 mm ISO.

The factors applied for the steel ladle lining optimization were the geometry (A), represented by the WL brick shape; IEA applied (B); and temperature (C), represented by the ILT. In Table 3, the optimization factors are outlined in detail.

**Table 3.** Optimization factors of the steel ladle lining.

Geometry	IEA		ILT [mm]		
A1	Brick 1	B1	IEA 1	C1	0
A2	Brick 2	B2	IEA 2	C2	3
A3	Brick 3	B3	IEA 3	C3	6
A4	Brick 4	B4	IEA 4	C4	9
		B5	IEA 5	C5	12

Simulations can provide results that do not meet the required conditions. Therefore, selection criteria (SC) were applied. SC 1 restricts the maximum SS temperature at the outer surface to  $\leq 400$  °C at the end of the idle time. To meet the second SC, the joint opening in the circumferential direction in 30 mm depth from the HF needs to be  $< 0.2$  mm at the end of preheating. This is a condition for securing closed joints at the beginning of the heat. A value of 0.2 mm represents closed joints between two bricks because tighter packing is impossible due to surface roughness. If the simulation results met both criteria, they were considered for optimization. This reduced the 100 lining configurations dataset to 42 for the VMC model and 43 when the DP criterion was applied (Figure 3). When both the criteria were met, the square was marked in green; a white square indicated that this criterion was fulfilled, and red square indicated that the simulation result did not meet the criterion. The optimization factors B5 (IEA of 0.63%) and C1 (0 mm ILT) were completely excluded.

### 2.3. TOPSIS

TOPSIS is a multiobjective decision-making method developed by Hwang and Yoon<sup>[19]</sup> and it is used to determine the best alternative among a set. Therefore, multiple responses are converted into a single response, represented by the relative closeness to the ideal solution ( $C^+$ ). The solution with the farthest and shortest Euclidean distance to the antiideal and ideal solutions, respectively, is called the best alternative. TOPSIS has already been applied to the ladle lining optimization<sup>[13]</sup> and other steelmaking-related topics.<sup>[20–23]</sup> Its implementation procedure is outlined in Figure 4 and consists of the following steps:

Step 1: Normalization of responses

$$\gamma_{ij} = \frac{Y_{ij}}{\sqrt{\sum_{i=1}^n Y_{ij}^2}} \quad (1)$$

where  $Y_{ij}$  is the normalized value of the  $j^{\text{th}}$  response in the alternative,  $Y_{ij}$  is the value of the  $j^{\text{th}}$  response in the  $i^{\text{th}}$  alternative, and  $N$  is the number of alternatives.

Step 2: Calculation of weighted normalized responses

$$v_{ij} = \gamma_{ij} \cdot w_j \quad (2)$$

where  $v_{ij}$  is the weighted normalized value of the  $j^{\text{th}}$  response in the  $i^{\text{th}}$  alternative,  $w_j$  is the weight of the  $j^{\text{th}}$  response, and  $\sum_{i=1}^n w_j = 1$  for a dataset with  $n$  responses.

Step 3: Determination of the ideal ( $A^+$ ) and anti-ideal ( $A^-$ ) solutions for “the lower, the better”-characteristic

$$A^+ = \{v_1^+, v_2^+, \dots, v_n^+\} = \min_{1 \leq i \leq N} (v_{ij}), \quad j = 1, 2, \dots, n \quad (3)$$

$$A^- = \{v_1^-, v_2^-, \dots, v_n^-\} = \max_{1 \leq i \leq N} (v_{ij}), \quad j = 1, 2, \dots, n \quad (4)$$

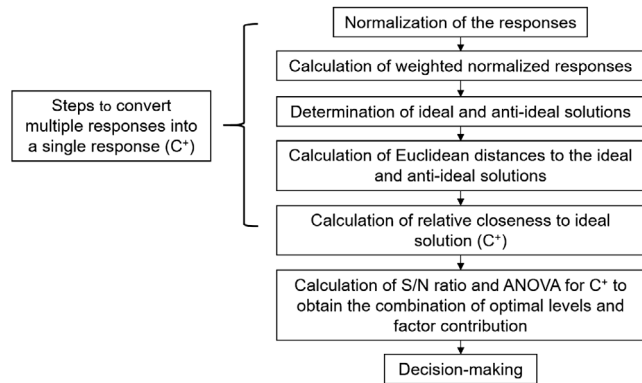
where  $v_n^+$  and  $v_n^-$  are the ideal and anti-ideal solutions of the  $n^{\text{th}}$  response, respectively;  $N$  is the number of alternatives; and  $n$  is the number of responses.

constitutive model: von Mises creep						
Brick		exp. Allow. 1	exp. Allow. 2	exp. Allow. 3	exp. Allow. 4	exp. Allow. 5
Expansion allowance in %		0.21%	0.32%	0.42%	0.53%	0.63%
		[mm]	[mm]	[mm]	[mm]	[mm]
Brick 1	SC1	█	█	█	█	█
	SC2	█	█	█	█	█
Brick 2	SC1	█	█	█	█	█
	SC2	█	█	█	█	█
Brick 3	SC1	█	█	█	█	█
	SC2	█	█	█	█	█
Brick 4	SC1	█	█	█	█	█
	SC2	█	█	█	█	█
		0 3 6 9 12	0 3 6 9 12	0 3 6 9 12	0 3 6 9 12	0 3 6 9 12
		Isolation layer thickness [mm]				

constitutive model: Drucker-Prager						
Brick		exp. Allow. 1	exp. Allow. 2	exp. Allow. 3	exp. Allow. 4	exp. Allow. 5
Expansion allowance in %		0.21%	0.32%	0.42%	0.53%	0.63%
		[mm]	[mm]	[mm]	[mm]	[mm]
Brick 1	SC1	█	█	█	█	█
	SC2	█	█	█	█	█
Brick 2	SC1	█	█	█	█	█
	SC2	█	█	█	█	█
Brick 3	SC1	█	█	█	█	█
	SC2	█	█	█	█	█
Brick 4	SC1	█	█	█	█	█
	SC2	█	█	█	█	█
		0 3 6 9 12	0 3 6 9 12	0 3 6 9 12	0 3 6 9 12	0 3 6 9 12
		Isolation layer thickness [mm]				

**Figure 3.** Simulation result datasets from: a) von Mises creep model, b) Drucker–Prager constitutive model when the SC were applied.



**Figure 4.** Flowchart of TOPSIS optimization procedure.

Step 4: Calculation of the Euclidian distances to the ideal ( $A^+$ ) and anti-ideal ( $A^-$ ) solutions

$$D_i^+ = \sqrt{\sum_{j=1}^n (v_{ij} - v_j^+)^2} \quad (5)$$

$$D_i^- = \sqrt{\sum_{j=1}^n (v_{ij} - v_j^-)^2} \quad (6)$$

Step 5: Calculation of the relative closeness to the ideal solution ( $C^+$ ) of each alternative

$$C_i^+ = \frac{D_i^-}{D_i^+ + D_i^-} \quad (7)$$

The alternatives are ranked according to the relative closeness to the ideal solution ( $C^+$ ). A high  $C^+$  value indicates a better performance, and the best alternative yields the highest  $C^+$  value.

## 2.4. Combination of Optimal Levels

$S/N$  ratios were calculated for the  $C^+$  values to obtain a combination of optimal levels. A higher  $C^+$  value indicates a better

lining performance, so  $C^+$  was evaluated with “the larger, the better” characteristic of Equation (8).<sup>[24]</sup> The optimal level yields the highest  $S/N$  ratio for each factor:

$$\frac{S}{N} = -10 \log \left( \frac{1}{m} \sum_{i=1}^m \frac{1}{Y_i^2} \right) \quad (8)$$

where  $m$  is the number of alternatives at one level of one factor, and  $Y_i$  is the value of the  $i^{\text{th}}$  alternative at one level of one factor.

## 3. Results and Discussion

The input datasets generated from the ladle lining simulation results were treated separately for the von Mises creep model and Drucker–Prager constitutive model. All the input values related to the lining data are outlined in Table 4. Lining case 20 of the VMC dataset was excluded due to the application of the SC.

### 3.1. Optimization Based on the Von Mises Creep Simulation Results

The responses were normalized using Equation (1), and equal-weighted normalized responses were calculated using Equation (2). Subsequently, the ideal and anti-ideal solutions were determined using Equation (3) and (4). The Euclidian distances of the alternative to ideal ( $D_i^+$ ) and anti-ideal ( $D_i^-$ ) solutions and the relative closeness to the ideal solution ( $C^+$ ) were calculated according to Equation (5)–(7), respectively. All the results are outlined in Table 5. The best steel-ladle lining case with the highest relative closeness  $C^+$  among the 42 cases was Case 14, utilizing Brick 2, an IEA of 0.25 mm and 9 mm of ILT (A2B1C4) (Figure 5). Several cases had  $C^+$  values very close to the best case, i.e., Case 14. A common feature of these cases was the application of the smallest IEA with 0.21% of the HF dimension.

The larger the better characteristics expressed by Equation (8) were used to calculate the  $S/N$  ratio of the  $C^+$ , as shown in Figure 6. The combination of the optimal levels was A2B1C2.

ANOVA was performed to evaluate the contributions of the individual factors. The contribution of each factor to  $C^+$  is shown

**Table 4.** Simulation results ( $\epsilon_{ir}$ ,  $x_{open}$ ,  $\vartheta_{ST}$ ).

Case	Brick shape	IEA [mm]	PL thickness [mm]	ILT [mm]	VMC			DP		
					$\epsilon_{ir}$ [-]	$x_{open}$ [mm]	$\vartheta_{ST}$ [°C]	$\epsilon_{ir}$ [-]	$x_{open}$ [mm]	$\vartheta_{ST}$ [°C]
1	1	0.2	70	6	-1.17 E-02	2.86 E-03	371.9	-1.15 E-02	9.01 E-02	371.9
2	1	0.2	67	9	-1.19 E-02	1.70 E-03	341.5	-1.19 E-02	9.08 E-02	341.5
3	1	0.2	64	12	-1.21 E-02	1.18 E-03	315.6	-1.22 E-02	8.76 E-02	315.6
4	1	0.3	70	6	-1.08 E-02	3.32 E-02	371.9	-1.02 E-02	8.79 E-02	371.9
5	1	0.3	67	9	-1.10 E-02	2.37 E-02	341.5	-1.06 E-02	8.57 E-02	341.5
6	1	0.3	64	12	-1.12 E-02	2.05 E-02	315.6	-1.09 E-02	8.71 E-02	315.6
7	1	0.4	70	6	-9.78 E-03	8.07 E-02	371.9	-8.76 E-03	9.53 E-02	371.9
8	1	0.4	67	9	-1.01 E-02	6.77 E-02	341.5	-9.30 E-03	8.90 E-02	341.5
9	1	0.4	64	12	-1.02 E-02	5.73 E-02	315.6	-9.63 E-03	8.60 E-02	315.6
10	1	0.5	67	9	-9.04 E-03	1.15 E-01	341.5	-8.04 E-03	1.21 E-01	341.5
11	1	0.5	64	12	-9.20 E-03	1.04 E-01	315.6	-8.19 E-03	1.13 E-01	315.6
12	2	0.25	104	3	-1.14 E-02	6.39 E-03	395.2	-1.13 E-02	1.10 E-01	395.2
13	2	0.25	101	6	-1.17 E-02	2.66 E-03	360.3	-1.18 E-02	1.05 E-01	360.3
14	2	0.25	98	9	-1.19 E-02	1.19 E-03	330.5	-1.21 E-02	1.00 E-01	330.5
15	2	0.25	95	12	-1.21 E-02	3.56 E-04	306.3	-1.23 E-02	9.65 E-02	306.3
16	2	0.38	104	3	-1.04 E-02	5.78 E-02	395.2	-1.00 E-02	1.18 E-01	395.2
17	2	0.38	101	6	-1.07 E-02	4.09 E-02	360.3	-1.05 E-02	1.14 E-01	360.3
18	2	0.38	98	9	-1.09 E-02	3.16 E-02	330.5	-1.08 E-02	1.10 E-01	330.5
19	2	0.38	95	12	-1.10 E-02	2.73 E-02	306.3	-1.11 E-02	1.07 E-01	306.3
20	2	0.51	104	3	-	-	-	-8.54 E-03	1.34 E-01	395.2
21	2	0.51	101	6	-9.67 E-03	1.03 E-01	360.3	-9.05 E-03	1.24 E-01	360.3
22	2	0.51	98	9	-9.80 E-03	9.04 E-02	330.5	-9.35 E-03	1.18 E-01	330.5
23	2	0.51	95	12	-1.00 E-02	8.04 E-02	306.3	-9.57 E-03	1.13 E-01	306.3
24	3	0.2	38	6	-1.17 E-02	2.88 E-03	383	-1.11 E-02	8.12 E-02	383
25	3	0.2	35	9	-1.20 E-02	1.07 E-03	351.9	-1.19 E-02	8.64 E-02	351.9
26	3	0.2	32	12	-1.22 E-02	8.21 E-04	323.9	-1.21 E-02	8.96 E-02	323.9
27	3	0.3	38	6	-1.09 E-02	3.57 E-02	383	-9.92 E-03	8.16 E-02	383
28	3	0.3	35	9	-1.11 E-02	2.17 E-02	351.9	-1.04 E-02	7.88 E-02	351.9
29	3	0.3	32	12	-1.13 E-02	1.69 E-02	323.9	-1.08 E-02	8.13 E-02	323.9
30	3	0.4	38	6	-9.98 E-03	8.31 E-02	383	-8.83 E-03	9.61 E-02	383
31	3	0.4	35	9	-9.03 E-03	6.57 E-02	351.9	-9.22 E-03	8.62 E-02	351.9
32	3	0.4	32	12	-1.05 E-02	5.18 E-02	323.9	-9.51 E-03	8.08 E-02	323.9
33	3	0.5	35	9	-9.28 E-03	1.13 E-01	351.9	-8.16 E-03	1.18 E-01	351.9
34	3	0.5	32	12	-9.55 E-03	9.88 E-02	323.9	-8.36 E-03	1.09 E-01	323.9
35	4	0.29	72.6	6	-1.15 E-02	3.45 E-03	371.6	-1.17 E-02	1.46 E-01	371.6
36	4	0.29	69.6	9	-1.18 E-02	1.94 E-03	341.2	-1.21 E-02	1.41 E-01	341.2
37	4	0.29	66.6	12	-1.20 E-02	1.25 E-03	315.3	-1.24 E-02	1.29 E-01	315.3
38	4	0.44	72.6	6	-1.05 E-02	4.57 E-02	371.6	-1.05 E-02	1.45 E-01	371.6
39	4	0.44	69.6	9	-1.07 E-02	3.14 E-02	341.2	-1.09 E-02	1.40 E-01	341.2
40	4	0.44	66.6	12	-1.09 E-02	2.66 E-02	315.3	-1.12 E-02	1.40 E-01	315.3
41	4	0.59	72.6	6	-9.33 E-03	1.22 E-01	371.6	-9.00 E-03	1.52 E-01	371.6
42	4	0.59	69.6	9	-9.57 E-03	1.03 E-01	341.2	-9.42 E-03	1.44 E-01	341.2
43	4	0.59	66.6	12	-9.86 E-03	8.78 E-02	315.3	-9.74 E-03	1.38 E-01	315.3

**Table 5.** Normalized responses  $\gamma_{ij}$ , weighted normalized responses  $\nu_{ij}$ ,  $D_i^+$ ,  $D_i^-$ , and  $C_i^+$  of the von mises creep input data.

Case	$\gamma_{ij}$			$\nu_{ij}$			$D_i^+$	$D_i^-$	$C_i^+$
	$\epsilon_{ir}$	$x_{open}$	$\vartheta_{ST}$	$\epsilon_{ir}$	$x_{open}$	$\vartheta_{ST}$			
1	-0.1673	0.0074	0.1662	-0.0552	0.0024	0.0548	0.0159	0.1023	0.8654
2	-0.1706	0.0044	0.1526	-0.0563	0.0015	0.0504	0.0145	0.1036	0.8768
3	-0.1733	0.0031	0.1410	-0.0572	0.0010	0.0465	0.0145	0.1043	0.8778
4	-0.1544	0.0863	0.1662	-0.0509	0.0285	0.0548	0.0309	0.0766	0.7125
5	-0.1575	0.0617	0.1526	-0.0520	0.0204	0.0504	0.0227	0.0849	0.7891
6	-0.1599	0.0532	0.1410	-0.0528	0.0175	0.0465	0.0200	0.0881	0.8150
7	-0.1403	0.2098	0.1662	-0.0463	0.0692	0.0548	0.0697	0.0374	0.3494
8	-0.1443	0.1760	0.1526	-0.0476	0.0581	0.0504	0.0582	0.0484	0.4538
9	-0.1467	0.1488	0.1410	-0.0484	0.0491	0.0465	0.0491	0.0576	0.5395
10	-0.1296	0.2983	0.1526	-0.0428	0.0984	0.0504	0.0983	0.0181	0.1558
11	-0.1319	0.2712	0.1410	-0.0435	0.0895	0.0465	0.0892	0.0239	0.2117
12	-0.1633	0.0166	0.1766	-0.0539	0.0055	0.0583	0.0180	0.0993	0.8468
13	-0.1675	0.0069	0.1610	-0.0553	0.0023	0.0531	0.0150	0.1026	0.8727
14	-0.1706	0.0031	0.1477	-0.0563	0.0010	0.0487	0.0140	0.1041	0.8813
15	-0.1729	0.0009	0.1369	-0.0571	0.0003	0.0452	0.0143	0.1052	0.8802
16	-0.1498	0.1503	0.1766	-0.0494	0.0496	0.0583	0.0514	0.0557	0.5200
17	-0.1533	0.1064	0.1610	-0.0506	0.0351	0.0531	0.0366	0.0701	0.6574
18	-0.1558	0.0821	0.1477	-0.0514	0.0271	0.0487	0.0284	0.0785	0.7344
19	-0.1581	0.0710	0.1369	-0.0522	0.0234	0.0452	0.0250	0.0825	0.7677
21	-0.1386	0.2673	0.1610	-0.0457	0.0882	0.0531	0.0883	0.0211	0.1927
22	-0.1406	0.2350	0.1477	-0.0464	0.0775	0.0487	0.0774	0.0310	0.2858
23	-0.1435	0.2091	0.1369	-0.0473	0.0690	0.0452	0.0688	0.0394	0.3642
24	-0.1680	0.0075	0.1712	-0.0554	0.0025	0.0565	0.0171	0.1023	0.8565
25	-0.1716	0.0028	0.1573	-0.0566	0.0009	0.0519	0.0154	0.1040	0.8708
26	-0.1752	0.0021	0.1447	-0.0578	0.0007	0.0478	0.0153	0.1045	0.8723
27	-0.1567	0.0927	0.1712	-0.0517	0.0306	0.0565	0.0335	0.0744	0.6892
28	-0.1597	0.0565	0.1573	-0.0527	0.0186	0.0519	0.0219	0.0864	0.7977
29	-0.1627	0.0441	0.1447	-0.0537	0.0145	0.0478	0.0181	0.0909	0.8337
30	-0.1431	0.2159	0.1712	-0.0472	0.0713	0.0565	0.0720	0.0351	0.3280
31	-0.1296	0.1708	0.1573	-0.0428	0.0564	0.0519	0.0565	0.0510	0.4748
32	-0.1504	0.1346	0.1447	-0.0496	0.0444	0.0478	0.0447	0.0617	0.5800
33	-0.1331	0.2931	0.1573	-0.0439	0.0967	0.0519	0.0967	0.0173	0.1515
34	-0.1370	0.2569	0.1447	-0.0452	0.0848	0.0478	0.0845	0.0258	0.2340
35	-0.1642	0.0090	0.1661	-0.0542	0.0030	0.0548	0.0152	0.1019	0.8702
36	-0.1687	0.0051	0.1525	-0.0557	0.0017	0.0503	0.0140	0.1034	0.8809
37	-0.1723	0.0033	0.1409	-0.0569	0.0011	0.0465	0.0142	0.1043	0.8802
38	-0.1499	0.1189	0.1661	-0.0495	0.0392	0.0548	0.0406	0.0661	0.6192
39	-0.1537	0.0816	0.1525	-0.0507	0.0269	0.0503	0.0283	0.0785	0.7353
40	-0.1570	0.0691	0.1409	-0.0518	0.0228	0.0465	0.0243	0.0830	0.7735
41	-0.1339	0.3173	0.1661	-0.0442	0.1047	0.0548	0.1048	0.0141	0.1185
42	-0.1372	0.2680	0.1525	-0.0453	0.0885	0.0503	0.0883	0.0220	0.1995
43	-0.1414	0.2281	0.1409	-0.0467	0.0753	0.0465	0.0751	0.0336	0.3091

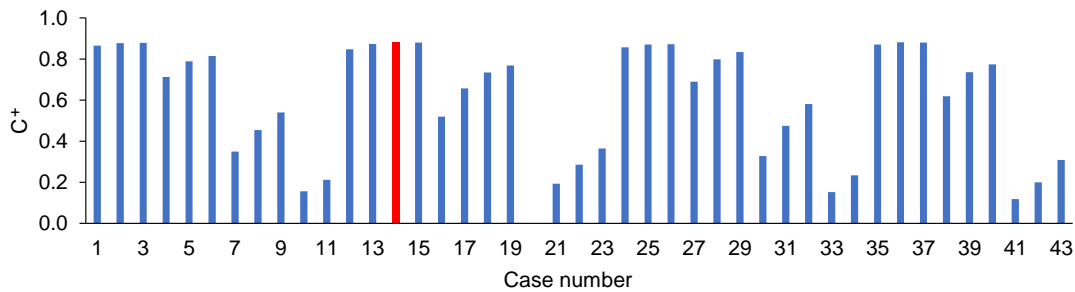


**Figure 5.**  $C^+$  for all cases of von Mises creep dataset.

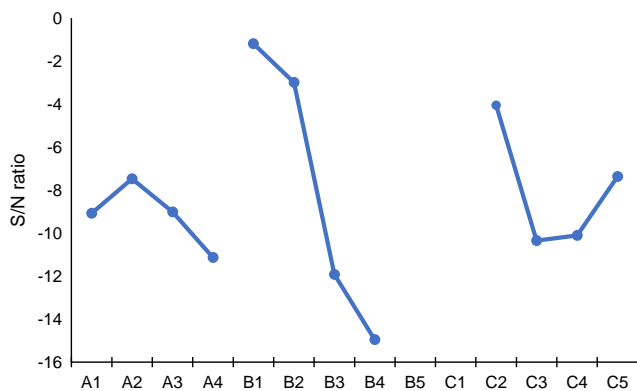


**Figure 6.** S/N ratio for  $C^+$  of the von Mises creep dataset.

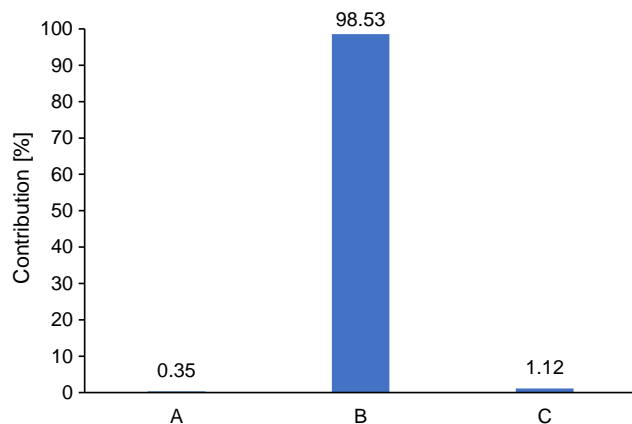


**Figure 7.** Contribution of individual factors to  $C^+$  of the von Mises creep dataset.

in **Figure 7**. Factor B, which was the IEA, made the most significant contribution to  $C^+$  (98.53%). Both the other factors have minor contributions, with 1.12% for C and 0.35% for A.

### 3.2. Optimization Based on the Drucker–Prager Simulation Results

The normalized responses, weighted normalized responses,  $D_i^+$ ,  $D_i^-$ , and  $C_i^+$  are listed in **Table 6**. The higher the relative

closeness  $C^+$ , the better the performance. **Figure 8** shows the rankings of the lining configurations. Case 32 provides the best performance among all the linings, consisting of Brick 3, 0.4 mm IEA, and 12 mm ILT (A3B3C5). The number of cases with a  $C^+$  value similar to that of the ideal case was lower than that of the VMC optimization. The cases representing the best performance for the DP criterion have a brick shape with low circumferential dimension, 0.4 mm IEA, and high ILT.

As shown in **Figure 9**, the combination of the optimal levels for  $C^+$  of the Drucker–Prager dataset was A3B4C5.

Similar to the von Mises dataset  $C^+$ , the statistical tool ANOVA was applied to quantitatively evaluate the main factors influencing the  $C^+$  in the Drucker–Prager dataset. The percentage contributions of each factor to the  $C^+$  are shown in **Figure 10**. The most significant contribution comes from Factor A (brick shape, 85.06%). Factors B and C, with percentages of 7.79% and 7.15%, respectively, still have a considerable contribution.

### 3.3. Comparison of the Lining Optimization Results

The TOPSIS results indicated significantly different ideal lining configurations for the material models. For the VMC simulations, the best solution was A1B1C4, whereas A3B3C5 was the ideal solution when the DP criterion was used. In comparison, the combination of optimal levels was A1B1C2 for VMC and A3B4C5 for DP. The results of the best solution and combination of optimal levels differed slightly. Both the results indicate that a brick shape with a larger circumferential dimension (WL HF width) combined with a small IEA is favorable for the VMC. If the DP criterion is applied, the favorable lining configuration consists of a brick shape with small circumferential dimension and IEA larger than that of the VMC. The most important factor influencing the  $C^+$  for the VMC was Factor B, the IEA, with 98.53%, compared to Factor A, the brick shape, which accounted for 85.06% in the case of DP.

The large difference in factor contribution between the VMC and DP criteria can be explained by the contribution of the constitutive models and is also indicated by the input value  $x_{open}$  (Table 4). The MgO-C material creep contributes above 800 °C, so during preheating up to 1000 °C, a considerable amount of creep strain manifests and increases the joint opening  $x_{open}$  until the end of preheating because temperatures in some distance of the HF increase. However, for the DP criterion, the failure line must be reached to trigger the irreversible strains. This occurs mainly

**Table 6.** Normalized responses  $\gamma_{ij}$ , weighted normalized responses  $\nu_{ij}$ ,  $D_i^+$ ,  $D_i^-$ , and  $C_i^+$  of the Drucker–Prager input data.

Case	$\gamma_{ij}$			$\nu_{ij}$			$D_i^+$	$D_i^-$	$C_i^+$
	$\epsilon_{ir}$	$x_{open}$	$\vartheta_{ST}$	$\epsilon_{ir}$	$x_{open}$	$\vartheta_{ST}$			
1	-0.1685	0.1246	0.1637	-0.0556	0.0411	0.0556	0.0201	0.0286	0.5871
2	-0.1746	0.1255	0.1503	-0.0576	0.0414	0.0511	0.0203	0.0290	0.5886
3	-0.1785	0.1212	0.1389	-0.0589	0.0400	0.0472	0.0205	0.0316	0.6061
4	-0.1497	0.1215	0.1637	-0.0494	0.0401	0.0556	0.0150	0.0311	0.6747
5	-0.1548	0.1185	0.1503	-0.0511	0.0391	0.0511	0.0137	0.0323	0.7023
6	-0.1596	0.1204	0.1389	-0.0527	0.0397	0.0472	0.0144	0.0326	0.6934
7	-0.1282	0.1318	0.1637	-0.0423	0.0435	0.0556	0.0128	0.0313	0.7091
8	-0.1360	0.1231	0.1503	-0.0449	0.0406	0.0511	0.0093	0.0332	0.7816
9	-0.1409	0.1189	0.1389	-0.0465	0.0392	0.0472	0.0084	0.0349	0.8054
10	-0.1177	0.1677	0.1503	-0.0388	0.0553	0.0511	0.0201	0.0264	0.5682
11	-0.1199	0.1557	0.1389	-0.0396	0.0514	0.0472	0.0155	0.0295	0.6555
12	-0.1656	0.1515	0.1739	-0.0547	0.0500	0.0591	0.0250	0.0199	0.4435
13	-0.1721	0.1457	0.1586	-0.0568	0.0481	0.0539	0.0231	0.0220	0.4871
14	-0.1765	0.1387	0.1454	-0.0582	0.0458	0.0495	0.0220	0.0254	0.5354
15	-0.1795	0.1335	0.1348	-0.0592	0.0441	0.0458	0.0219	0.0284	0.5644
16	-0.1469	0.1626	0.1739	-0.0485	0.0536	0.0591	0.0241	0.0192	0.4437
17	-0.1531	0.1576	0.1586	-0.0505	0.0520	0.0539	0.0214	0.0202	0.4853
18	-0.1573	0.1515	0.1454	-0.0519	0.0500	0.0495	0.0195	0.0229	0.5399
19	-0.1624	0.1476	0.1348	-0.0536	0.0487	0.0458	0.0195	0.0252	0.5639
20	-0.1250	0.1853	0.1739	-0.0412	0.0612	0.0591	0.0286	0.0202	0.4145
21	-0.1325	0.1715	0.1586	-0.0437	0.0566	0.0539	0.0227	0.0211	0.4821
22	-0.1368	0.1627	0.1454	-0.0451	0.0537	0.0495	0.0192	0.0234	0.5504
23	-0.1401	0.1565	0.1348	-0.0462	0.0517	0.0458	0.0173	0.0259	0.5989
24	-0.1628	0.1123	0.1685	-0.0537	0.0370	0.0573	0.0188	0.0328	0.6350
25	-0.1736	0.1195	0.1549	-0.0573	0.0394	0.0527	0.0200	0.0306	0.6049
26	-0.1768	0.1239	0.1425	-0.0583	0.0409	0.0485	0.0203	0.0303	0.5990
27	-0.1451	0.1128	0.1685	-0.0479	0.0372	0.0573	0.0147	0.0342	0.6996
28	-0.1518	0.1090	0.1549	-0.0501	0.0360	0.0527	0.0132	0.0352	0.7279
29	-0.1580	0.1124	0.1425	-0.0521	0.0371	0.0485	0.0136	0.0347	0.7186
30	-0.1292	0.1330	0.1685	-0.0426	0.0439	0.0573	0.0144	0.0307	0.6798
31	-0.1349	0.1192	0.1549	-0.0445	0.0393	0.0527	0.0095	0.0342	0.7825
32	-0.1392	0.1118	0.1425	-0.0459	0.0369	0.0485	0.0076	0.0368	0.8285
33	-0.1193	0.1634	0.1549	-0.0394	0.0539	0.0527	0.0192	0.0263	0.5780
34	-0.1223	0.1511	0.1425	-0.0404	0.0499	0.0485	0.0142	0.0294	0.6739
35	-0.1717	0.2024	0.1635	-0.0567	0.0668	0.0556	0.0369	0.0053	0.1258
36	-0.1771	0.1947	0.1501	-0.0584	0.0642	0.0511	0.0348	0.0096	0.2158
37	-0.1813	0.1785	0.1388	-0.0598	0.0589	0.0472	0.0311	0.0158	0.3365
38	-0.1538	0.2009	0.1635	-0.0507	0.0663	0.0556	0.0340	0.0102	0.2299
39	-0.1588	0.1937	0.1501	-0.0524	0.0639	0.0511	0.0315	0.0122	0.2784
40	-0.1633	0.1933	0.1388	-0.0539	0.0638	0.0472	0.0317	0.0144	0.3127
41	-0.1317	0.2097	0.1635	-0.0435	0.0692	0.0556	0.0349	0.0167	0.3239
42	-0.1379	0.1993	0.1501	-0.0455	0.0658	0.0511	0.0310	0.0168	0.3515
43	-0.1425	0.1915	0.1388	-0.0470	0.0632	0.0472	0.0284	0.0185	0.3944



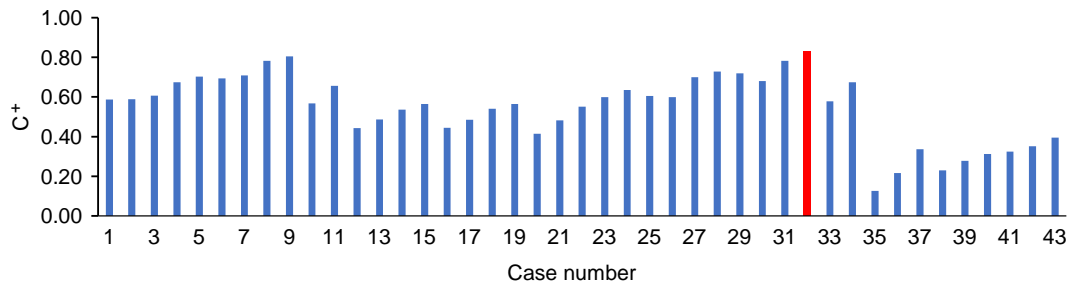


**Figure 8.**  $C^+$  for all cases of the Drucker–Prager dataset.

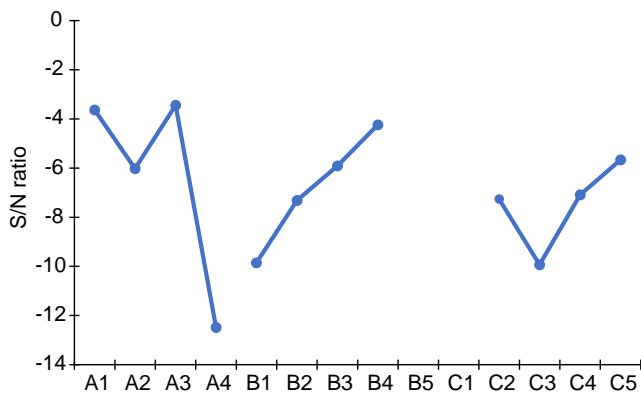


**Figure 9.** S/N ratio for  $C^+$  of the dataset.

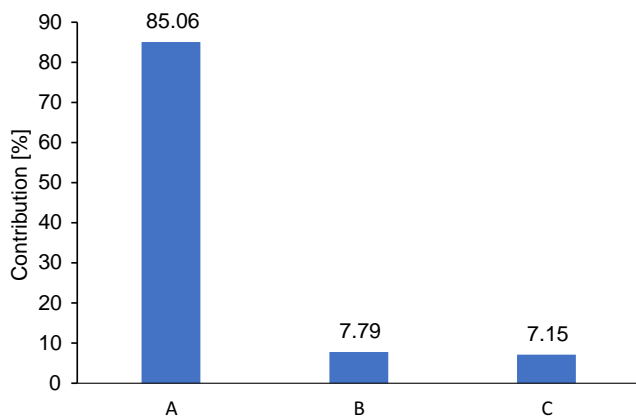


**Figure 10.** Contribution of individual factors to  $C^+$  of the dataset.

during the thermal shock; therefore, the DP criterion does not contribute irreversible strains during preheating.

The  $x_{open}$  results can be distinguished based on the circumferential dimensions. For the bricks with small circumferential dimensions (Bricks 1 and 3), the relative difference in  $x_{open}$  between the IEA 1 and IEA 4 was high ( $0.002 \rightarrow 0.11$  mm) and similar for both the constitutive models. For bricks with large circumferential dimensions (Bricks 2 and 4), the  $x_{open}$  results were different for the material models. For the VMC simulations, the results were similar to those for bricks with small circumferential dimensions. For the DP model, the relative difference is small ( $0.09 \rightarrow 0.13$  mm). Since input parameters with

large relative differences affect the results more, it follows that the IEA for VMC and the brick geometry for DP are the determining factors.

A more simplified input parameter set utilizing the irreversible strain and SS temperature would display similar optimum designs for both constitutive models (i.e., the highest insulation and the highest expansion allowance), and only the percentages of the contribution factors would differ slightly.

#### 4. Conclusion

TOPSIS was successfully applied to optimize a steel ladle slag zone lining by considering commercial refractory materials, a measured temperature program, and irreversible material behavior. For the applied constitutive models, VMC and DP, the optimal lining configurations differed significantly. A lining optimized using the VMC simulation data has a brick with a large circumferential dimension and no or only a small IEA. The main factor influencing the contribution of 98.53% was Factor B, IEA. Bricks with a small circumferential dimension combined with an IEA larger than that for the VMC yield the optimized lining configuration according to the DP simulation data. With 85.06% of Factor A, the brick shape was the main contributor. Because the ladle lining is a very complex system, these results help to improve the understanding of the optimal refractory lining design.

Comprehending the failure mechanisms, whether time-dependent or time-independent, holds pivotal importance in optimizing and designing refractory linings. In the case of the presented MgO-C material, notable creep failure manifests prominently at 800 °C, inducing considerable creep strain during preheating. Typically, the DP failure line is reached during thermal shock, leading to minimal irreversible strains in the preheating phase. Consequently, the impact of constitutive models varies distinctly across different timeframes, greatly influenced by material properties and subject to alteration based on the specific refractory material employed. In the case, the DP failure line cannot be reached, creep failure is the main contributor in the high-temperature region.

Further adaptation of the optimization procedure, such as applying different weights or weighting methods to the input data, should be considered. In addition, a combined material model that considers the DP and VMC in the elastic region would be advantageous. The results for linings with a constant IEA could also be valuable as well, as it may be difficult to apply

the exact IEA from a practical point of view. In future investigations, the lining configuration obtained by the optimization procedure should be validated by experimental trials in a dedicated testing furnace.

## Acknowledgements

The authors gratefully acknowledge the funding support of K1-MET GmbH, metallurgical competence center. The research program of the K1-MET competence center is supported by COMET (Competence Center for Excellent Technologies), the Austrian program for competence centers. COMET is funded by the Federal Ministry for Climate Action, Environment, Energy, Mobility, Innovation, and Technology, the Federal Ministry for Labour and Economy, the Federal States of Upper Austria, Tyrol, and Styria as well as the Styrian Business Promotion Agency (SFG) and the Standortagentur Tyrol. Furthermore, Upper Austrian Research GmbH continuously supports K1-MET. Besides the public funding from COMET, this research project is partially financed by the scientific partner Montanuniversität Leoben and the industrial partners RHI Magnesita GmbH, voestalpine Böhler Edelstahl GmbH and voestalpine Stahl GmbH.

## Conflict of Interest

The authors declare no conflict of interest.

## Data Availability Statement

The data that support the findings of this study are available from the corresponding author upon reasonable request.

## Keywords

lining optimization, magnesia carbon refractory, slag zone, steel ladles, technique for order preference by similarity to the ideal solution

Received: August 21, 2023

Revised: February 28, 2024

Published online: March 13, 2024

- [1] T. Vert, *Refractory Material Selection for Steelmaking*, The American Ceramic Society Wiley, Hoboken, NJ **2016**.
- [2] D. H. Hubble, R. O. Russell, H. L. Vernon, R. J. Marr, *Steelmaking and Refining Volume*, The AISE Steel Foundation, Pittsburgh **1998**.
- [3] S. Samadi, S. Jin, D. Gruber, H. Harmuth, *Finite Elem. Anal. Des.* **2022**, *206*, 103762.
- [4] D. Gruber, H. Harmuth, *Steel Res. Int.* **2014**, *85*, 512.
- [5] D. Gruber, *Steel Res. Int.* **2008**, *79*, 913.
- [6] S. Jin, T. Auer, D. Gruber, H. Harmuth, M. H. Fréchet, Y. Li, *Interceram/Refractories Manual* **2012**, pp. 37–41.
- [7] W. Cheng, Y. Sun, G. Li, J. Kong, G. Jiang, Z. Li, *Appl. Math. Inf. Sci.* **2017**, *11*, 611.
- [8] M. F. Santos, M. H. Moreira, M. G. G. Campos, P. I. B. G. B. Pelissari, R. A. Angélico, E. Y. Sako, *Ceram. Int.* **2018**, *44*, 12831.
- [9] M. Ali, T. Sayet, A. Gasser, E. Blond, *Ceramics* **2020**, *3*, 171.
- [10] G. Li, J. Liu, G. Jiang, H. Liu, *Adv. Mech. Eng.* **2015**, *7*, 168781401557598.
- [11] A. Hou, S. Jin, H. Harmuth, D. Gruber, *Steel Res. Int.* **2019**, *90*, 1900116.
- [12] A. Hou, S. Jin, H. Harmuth, D. Gruber, *JOM* **2018**, *70*, 2449.
- [13] A. Hou, D. Gruber, S. Jin, *Steel Res. Int.* **2023**, *94*, 2200407.
- [14] *ABAQUS: Standard User's Manual*, Dassault Systèmes Simulia Corp, Providence, RI **2019**.
- [15] S. Fuchshumer, G. Grimm, S. Natschläger, R. Rössler, H. Seyrkammer, in *Proc. 9th Int. Conf. Modeling and Simulation of Metallurgical Processes in Steelmaking*, ASMET, Leoben, Austria **2021**.
- [16] *VDI-Wärmeatlas*, Springer Berlin Heidelberg, Berlin, Heidelberg **2013**.
- [17] M. Stueckelschweiger, D. Gruber, S. Jin, H. Harmuth, *Ceram. Int.* **2019**, *45*, 9776.
- [18] D. C. Drucker, W. Prager, *Q. Appl. Math.* **1952**, *10*, 157.
- [19] *Multiple Attribute Decision Making: Lecture Notes in Economics and Mathematical Systems* (Eds: C. L. Hwang, K. Yoon), Springer, Berlin, Heidelberg **1981**.
- [20] D. P. Santos, P. I. B. G. B. Pelissari, B. S. Oliveira, D. R. Leiva, R. F. Mello, V. C. Pandolfelli, *Ceram. Int.* **2020**, *46*, 4113.
- [21] A. Rayhanizadeh, N. Towhidi, S. Ebrahimnejad, Y. Shajari, *Eng. Res. Express* **2020**, *2*, 25009.
- [22] Y. Li, H. Li, J. Zhang, S. Zhang, Y. Yin, *IEEE Access* **2020**, *8*, 35712.
- [23] S. Kumar, A. G. Barman, *Soft Comput.* **2021**, *25*, 6505.
- [24] R. K. Roy, *A Primer on the Taguchi Method*, 2nd ed., Society of Manufacturing Engineers, Dearborn, MI **2010**.
- [25] M. Klopff, D. Gruber, *Open Ceram.* **2023**, *14*, 100369.